



Spatial variation of the source mechanisms in the Egyptian continental margin

Iman F. Abu El Nader ¹, Asem Salama ¹, Mohamed N. El-Gabry ²,
Hesham M. Hussein ^{1, 2} and Mona Abdelazim ²

¹ General Seismology Lab, Seismology Department, National Research Institute of Astronomy and Geophysics (NRIAG), Helwan, Cairo, Egypt

² Egyptian National Data Center (ENDC), National Research Institute of Astronomy and Geophysics (NRIAG), Helwan, Cairo, Egypt

Received 29 July 2023, in final form 25 June 2024

The spatial variability of the focal mechanism solutions in the NW Egypt Cyrenaica and Levant-north Egypt domains of the Egyptian Continental margin is investigated based on the polarity of the P-wave first motions of eleven earthquakes with local magnitudes M_L ranging from 4.2 to 6.2. The identified focal mechanism solutions in the Levant-north Egypt domain are evaluated in two sub-provinces with different geological settings. The first sub-province shows strike-slip faulting mechanisms with right-lateral motion along the NE-trending Rosetta-Qattara fault zone, while the NW-trending Tamsah fault zone produces left-lateral strike-slip motion. The inland extension of the Rosetta-Qattara fault zone towards the Western Desert reflects the same sense of motion. Strike-slip faulting with thrust components dominates the focal mechanisms in the second sub-province but with a different stress orientation. A single thrust faulting mechanism event which occurred on the periphery of the continental shelf shows the same common orientation of the stress field at the Hellenic Arc. This type of mechanism in this locality can be explained by the mean of compressional stress transfer towards the coast generated by the accelerated southwest retreat of the Hellenic Trench. The complex regional stress along the Cyprian and Hellenic arcs, the current local structure features, and the dominant orientation of the pre-existing fault are the factors that contribute to the changeable stress pattern field in the Levant-north Egypt domain. A single event in the second domain, the NW Egypt Cyrenaica, is a strike-slip with a right-lateral sense of motion on a WNW-oriented plane, consistent with motion along the WNW tectonic fault which separates the continental shelf from the oceanic crust.

Keywords: Egyptian continental margin, focal mechanisms, Rosetta – Qattara fault, passive margin

1. Introduction

Compared to passive continental margins, active plate boundaries record most earthquakes. Mann (2015) defined the passive margins as sedimentary wedges that overlie an inactive and subsiding weld between rifted continental crusts and the newly formed oceanic crust of the main Wilson cycle of ocean opening. Their deformation ages are vital indicators of opening and closing processes through geological time. Johnston (1989) investigated global passive continental margin earthquakes that are believed to be related to the tectonic features of the stable continental zone. He concluded that the passive continental margins produced by intra-continental rifting extension are currently subjected to compressional stresses. As a result, strike-slip and thrust earthquakes are more common, indicating that the original, normal faults have been reversed. Faults created during rifting continue as zones of weakness for an extended period, even when the stress regime turns into compression (Caméra et al., 2010; Holdsworth et al., 2001; Brune et al., 2014).

The interaction of the African, Arabian, and Eurasian tectonic plates and other microplates, such as the Anatolian and Aegean, significantly affects the tectonics of the Egyptian continental margin (Fig. 1). The deformation in this area is the result of African Plate subduction towards the north, the Arabian Plate moving towards the Eurasian plate in a north-northwest direction (Rosenbaum et al., 2002), the westward pushing out of the Aegean–Anatolian micro-plate, marked by the existence of Anatolian fault zones both in the east and the north (Le Pichon et al., 1988; McClusky et al., 2003). According to Maamoun et al. (1984) there is only minor scattered activity over the Egyptian continental margin. September 12, 1955 ($M_L = 6.2$), May 28, 1998 ($M_L = 5.9$), and January 30, 1951 ($M_L = 5.6$) Levantine basin events were the three significant earthquakes that affected the margin between 1900 and 2011. Two significant historical events occurred in the margin in 320 AD and 956 AD, respectively. According to Korrat et al. (2005) both earthquakes originated north of the $M_L = 6.2$ September 12, 1955 earthquake. Later, some moderate-sized earthquakes with local magnitudes of M_L 5.1, 4.8, 4.2, 5.1, 4.8, and 4.3 occurred in the Egyptian continental margin and nearby onshore areas on October 19, 2012, January 17, 2013, September 3, 2015, May 15, 2019, July 05, 2019, and April 11, 2020, respectively, according to the ISC bulletin.

Many digital waveform data were made available by the seismological networks that have grown over the past 20 years in Egypt and worldwide. These networks make it possible to record small earthquakes with good azimuth coverage, which contributes to creating extra focal mechanisms. We made use of three programs from Seisan 2.5 (Havskov et al., 2020): FOCMEC (Snoke et al., 1984), HASH (Hardebeck and Shearer, 2008), and PINV (Suetsugu, 1998) to construct the focal mechanism solutions. In this study, focal mechanism solutions for eleven earthquakes with $M_L \geq 4.2$, which occurred along the Egyptian continental margin, have been constructed to

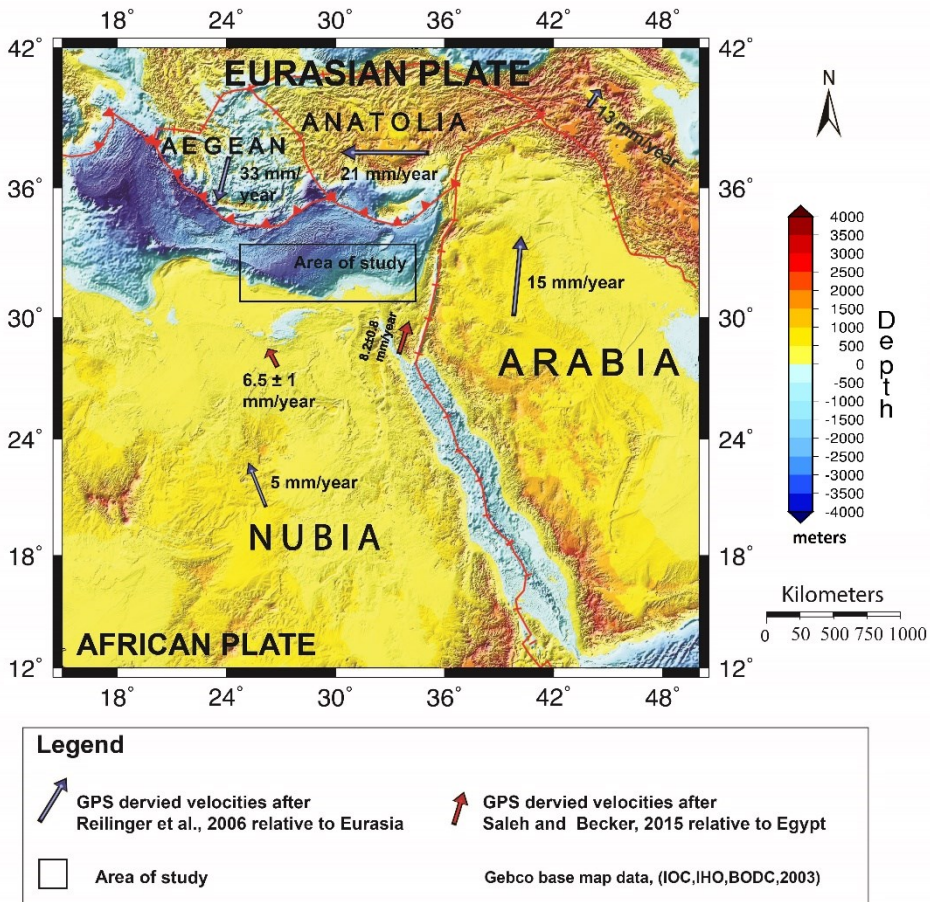


Figure 1. The tectonic movements of major tectonic plates (African, Arabian, and Eurasian) and microplates (Anatolian and Aegean) referenced to the Egyptian continental margin studied area.

identify the spatial variations of the faulting type in the Egyptian margin. The parameters of the new solutions have been briefly addressed regarding the local geological context. This work may enhance our understanding of neotectonics in this area.

2. Tectonic setting

The geodynamics of the eastern Mediterranean is characterized by the combined effects of the interplay between active subduction of Africa beneath Eurasia along the eastern Hellenic and Cypriot arcs, the active deformation along the Dead Sea-Levant and eastern Anatolia transcurrent fault zones as a result of the relative movement of the Arabian plate with respect to Africa

and the Suez Trench, and the Egyptian continental margin lying south of the eastern Mediterranean (McKenzie, 1972; Neev, 1975; Courtillot et al., 1987; Sage and Letouzey, 1990; Le Pichon et al., 1995; Mascle et al., 2000; McClusky et al., 2000). As a result of the interaction between the Hellenic arc trench retreat and Anatolia escaping, the trench has retreated up to 3 cm y^{-1} in the southwest direction. The Hellenic and Cyprian arcs have manifested different natures of convergence. The Cyprian Arc, which is approximately half the length of the Hellenic Arc, is affected by collision, subduction, and transcurrent movements, while the Hellenic Arc is affected by subduction along its entire length. In conclusion, the two arcs exhibit considerable variations in their relative motion throughout the arcs, both in terms of rate and direction (Wdowinski et al., 2006).

The seafloor of the margin has been dominated by the existence of the Herodotus Basin, Mediterranean Ridge accretionary complex, Nile Deep-Sea Fan, and Eratosthenes Seamount. According to surface wave tomography studies, the Egyptian margin is thought to be a thin crustal thickness continental margin, while the Herodotus Basin is mainly underlain by oceanic crust (El-Gabry et al., 2012; El-Sharkawy et al., 2021). The following significant tectonic events governed the structural evolution of the Egyptian continental margin:

- 1) the Neo-Tethyan rifting phase during the early Mesozoic,
- 2) the Late Cretaceous (Late Santonian)-Tertiary convergence movement of both African and Eurasian plates.

The Neo-Tethyan rifting phase, which began with the opening of Neotethys and the divergent motion of the Afro-Arabian and Eurasian plates, is the Early Mesozoic-Cenozoic tectonic phase that has a significant effect on the Egyptian margin (Robertson and Dixon, 1984; Moustafa and Khalil, 1994; Moustafa, 2020). The Late Triassic marks the beginning of this phase with obliquely divergent NW-SE extensional tectonic activity, which continued until the Early Cretaceous. It led to the formation of two offshore passive morphological domains: the orthogonally rifted Levant–north Egyptian continental margin and the obliquely divergent NW Egyptian–Cyrenaica margin (Jagger et al., 2018). The Levant–North Egyptian domain extends from the Cyprian Arc offshore Syria to the northern continental shelf of Egypt beneath the Western Nile cone. This domain is distinguished by thinned and rifted continental crust that is lower than 25 km thick. This form of crust extends approximately 400 km between the continental shelf and the Herodotus and Ionian abyssal plains, where it meets the oceanic crust, which is 5–9 km thick (*e.g.* Ben-Avraham et al., 2002; Marone et al., 2003; Cowie and Kuszniir, 2012a, b). The opening of the Neo-Tethys during the early Mesozoic has led to the formation of the NE-SW trending Rosetta-Qattara fault zone, which extends through the southwestern Western Desert, and the NW-SE

trending Tamsah fault zone in this domain (Abd El-Fattah et al., 2021). The NE-SW trending Rosetta fault separates the western Nile Cone border from the eastern border of Herodotus Basin, stretching for 200 Km and dipping to NNW (Eyal and Reches, 1983; Moustafa, 2020; Abd El-Fattah et al., 2021). It is regarded to be one of those NE-SW trending rift parallel faults created in the Herodotus basin and onshore extensional basins during the Neo-Tethyan rifting phase (Abd El-Fattah, 2018; Abd El-Fattah et al., 2021). It was characterized by a normal slip in the early Mesozoic time. According to Cowie and Kusznir (2012a), the Levant basin has structural highs such as Eratosthenes Seamount, which are bordered by normal faults that have the same orientation as the Rosetta fault as well as NE-SW and NNE-SSW trending normal faults mapped from seismic reflection data (Peace et al., 2012). Additionally, these faults also demonstrate the history of early Mesozoic extension. These extensional fault systems are disconnected and displaced along their strike by a set of NW–SE trending linear structures that were thought to be transfer or accommodation zones (Jagger et al., 2018). The NW-SE trending Tamsah Fault is parallel to these linear structures. The NW-trending Tamsah fault is another fault trend that is also cutting across the Levant–north Egyptian margin to the south of Eratosthenes Seamount and superimposes a deeper basement fault (Masclé et al., 2001; Dolson et al., 2014). The elevated thick Eratosthenes seamount that exists to the NNE of the Levant–North Egyptian domain interrupts the collision between Africa and Anatolia (Kempfer, 1998). The Cyprian Arc and Eratosthenes Seamount colliding could cause transmission of the plate boundary stress southward, reactivating the pre-existing passive margin fault zone (Ben-Avraham and Nur, 1987).

The domain of the NW Egyptian–Cyrenaica (Fig. 2) expands from the offshore Western Desert, western Nile Delta, to the offshore Cyrenaica Platform in NE Libya. This domain exhibits a sudden transition from the rifted continental crust, 30 km thick in the shelf region, to highly thinned and faulted continental–transitional crust, 22 km below the outer continental shelf, and then to idealistic oceanic crust, 5–9 km thick, underlying the Herodotus and Ionian abyssal plains (*e.g.* Brönnner and Makris, 2000; Marone et al., 2003). This transition is distinguished by the existence of WNW trending highly faulted narrow zone that displays some features of the transform margin (*e.g.*, Bird, 2001; Nemčok et al., 2016). This fault system is characterized by right-lateral strike-slip motion (Ben-Avraham et al., 1987). The NW Egyptian–Cyrenaica domain of the margin collides with the accretionary outer domain of the major arc-shaped Mediterranean ridge (Jagger et al., 2018). The Mediterranean ridge constitutes the submerged leading edge of the extended African margin (Brönnner and Makris, 2000). The outer and axial Mediterranean Ridge experiences mainly compression with major back thrust fault zones between them (Masclé and Chaumillon, 1998). The outer domain

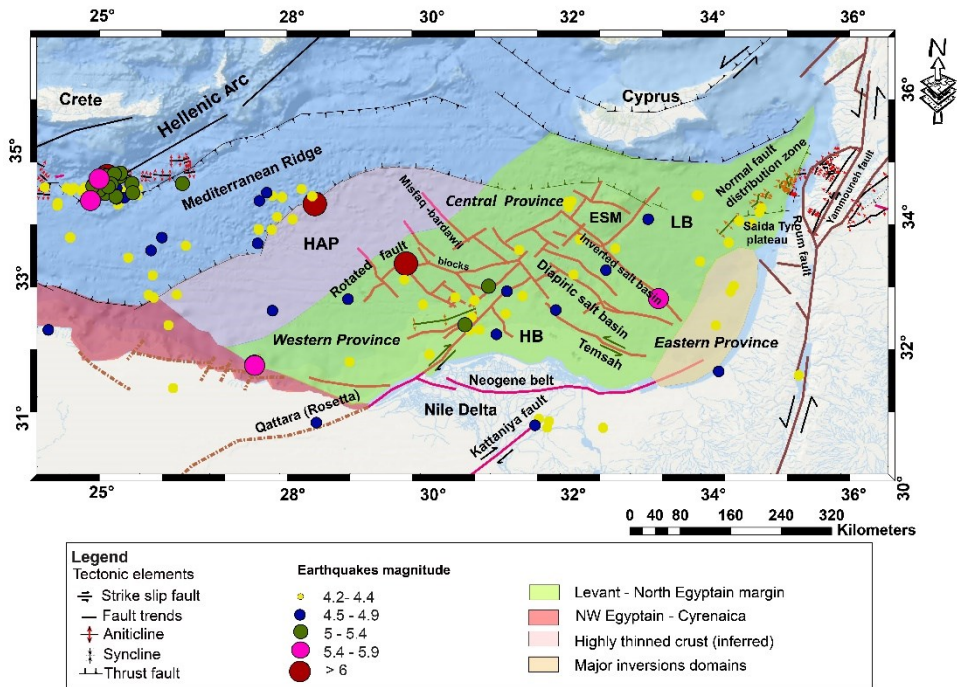


Figure 2. Tectonic elements and seismicity ($4.2 \leq ML \leq 6.0$) from ISC bulletin along the Egyptian continental margin. Faults offshore and onshore delta are compiled from Abdel Aal et al. (2000) and Loncke et al. (2006) (traced in red). Dead Sea fault system and Levantine Province are compiled from Ghalayini et al. (2014) and Jagger et al. (2018) (traced in green). The Mediterranean Ridge fault system is compiled from Barrier et al. (2004) and Tassy et al. (2015) (black). Rosetta Qattara fault is from Dolson et al. (2014). The abbreviation HAP stands for Herodotus Abyssal Plain, HB is for Herodotus Basin, LB is for the Levant Basin, and ESM is for Eratosthenes Seamount.

of the ridge is in contact with the interrupted segments of the Herodotus basin at the edge of the Egyptian continental margin (Huguen et al., 2006), while the Hellenic trench borders the ridge from the north.

The tectonic event occurred in Late Cretaceous (Late Santonian)-Tertiary convergence movement of both African and Eurasian plates resulted in the closure of New-Tethys (Moustafa, 2020). The resulting pre-Messinian compressional stress reactivated the Rosetta-Qattara fault by reverse slip, exhibiting positive structure inversion of the Mesozoic extensional basin and causing the creation of asymmetric anticline that affected the Tortonian and older sediments through the southern part of the hanging wall of this fault (Fig. 2), (Eyal and Reches, 1983; Abd El Fattah et al., 2021). Onshore positive inverted structures have indicated that transpressive stress might form this inversion with a small dextral slip component, indicating a possible WNW-ESE convergence direction (Orwing, 1980; Abdel-Aal et al., 2001). The Rosetta fault experienced two short-term episodes of left lateral trans tension within

the Messinian and Holocene epochs; however, between these two phases, the Rosetta-Qattara fault experienced normal dip-slip motion (Abd El Fattah et al., 2021). During these extensional and trans tensional periods, the area of the Herodotus basin northwest of the Rosetta fault suffered from NW-SE shortening, as demonstrated by the creation of NE-SW oriented folds (Moustafa, 2020; Abd El Fattah et al., 2021). This deformation pattern may be attributed to changes in the orientation of the converging plate boundary from NE-SW on the northwestern border of the Herodotus basin (SE of Crete) to E-W south of Cyprus. The axis of the maximum horizontal stress in the Herodotus Basin is presently directed at NNW-SSE (Heidbach et al., 2016).

During the second tectonic phase, the Tamsah fault was positively reactivated by reverse slip, exhibiting positively inverted Oligocene age normal slips as a result of compressional stress brought by the continuous convergence of African and Eurasian plates (Dolson et al., 2014; Hussein, 2013). The compressional stress in the Miocene and recent times also created NW to WNW trending detachment Oligo-Miocene folds in the area above the Tamsah fault zone (Moustafa, 2020). In Pliocene, the Tamsah trend (Fig. 2) showed strike-slip tectonic activity, which may be attributed to trans tensive stress (Abdel-Aal et al. 2001, El Barkooky and Helal. 2002).

3. Seismicity of the continental margin

The geographical distribution of earthquakes throughout the continental margin of Egypt with local magnitudes M_L ranging from 4.2 to 6.2 was compiled from the bulletins of the International Seismological Center (ISC) and the Egyptian National Seismological Network (ENSN) between 1900 and 2020 (Fig. 2). This figure shows that the earthquake activity in the margin is scattered. The local magnitudes of the studied earthquakes have been extracted from the ISC bulletin. Table 1 briefly summarizes the felt earthquakes that struck the Egyptian continental margin, including the M_L 5.6, 6.2, and 5.9 earthquakes that occurred on January 30, 1951, September 12, 1955, and May 28, 1998, respectively. These events took place on the Levant–north Egyptian continental margin domain. On April 9, 1987, and June 9, 1988, two further earthquakes with local magnitudes of 4.4 and 4.5 also struck the Levant–north Egyptian continental margin domain. In the last ten years, three earthquakes, including those on October 19, 2012, January 17, 2013, and July 5, 2019, events occurred on the Levant-north Egyptian margin along the NE trending Rosetta-Qattara fault zone and the associated sub-parallel faults with local magnitudes M_L 5.1, 4.8 and 4.8 respectively. This fault system cut across the western part of the Levant–north Egyptian margin. On May 15, 2019, an earthquake with magnitude $M_L = 5.1$ also occurred on the 2019, an earthquake with magnitude $M_L = 5.1$ also occurred on the

Table 1. Information about the felt earthquakes in the Egyptian continental margin.

YYYYMMDD	Location		Descriptions	References
	Lat.	Long.		
19510130	32.3725	33.4537	This event has been located to the north of the Nile Delta on the Egyptian margin. Few people felt this event in Cairo with intensity II. At Port Said, it was rather strong, frightening sleepers with intensity V. The shock was also felt in Israel as a whole, which in some places caused people to run outdoors, without damage. In south Lebanon, it has been rarely noticeable.	Ambraseys et al. (2005)
19550912	32.4183	29.7483	This earthquake is the largest documented one in the Egyptian continental margin. This earthquake caused widespread damage in the Nile Delta between Cairo and Alexandria. It was felt as far as Asyut to the south with an intensity ranging from III to VIII in Egypt. In the province of Bahira, a maximum intensity of VII-VIII has been reported where five people have been killed and 61 injured. Three hundred older brick buildings have been destroyed on the western side of the Nile Delta. In all of Egypt, 18 people were killed, 89 were injured, 40 houses collapsed completely and about 420 were ruined. This earthquake has been also felt throughout the Eastern Mediterranean, in Palestine, Cyprus, Crete, the island of Dodecanese and Athens.	Ambraseys et al. (2005) Al-Ahram Egyptian journal
19980528	31.4010	27.6670	This event struck the continental shelf periphery. Based on the long observation period, there was a lack of moderate magnitude earthquakes ($M_L \geq 5$) in this area before the 1998 event. The maximum MM intensity produced by this event (VII) was designated to Ras El-Hikma which is located about 50 km from the event. Alexandria City experienced an intensity of V-VI. The 1998 earthquake felt as far as Nicosia and Cyprus with an Intensity of II-MM.	Hassoup and Tealeb (2000)

Levant-north Egyptian margin, along with one of the sub-parallel faults to the NNW- SSE trending Temsah main fault. This event represents the largest among the limited number of small-magnitude earthquakes that happened in the Temsah fault zone. Onshore along the Alamein fault in the southwestern Western Desert, which is the extension of the Rosetta-Qattara fault, the earthquake of September 3, 2015, with $M_L=4.2$ occurred. The most recent event is the $M_L=4.3$ earthquake that occurred on April 11, 2020, along one of the WNW-ESE trending faults existing along the NW Egypt-Cyrenaica margin.

4. Data and methods

The polarity data were picked manually by carefully investigating the digitally recorded waveforms from the Egyptian National Seismological Network and four stations from the International Data Center of the Comprehensive Test Ban Treaty Organization (CTBTO) as well as the available polarities in the International Seismological Center (ISC) bulletin for events occurring between 2012 and 2020. Polarity data for the events before 2012 were gathered directly from the International Seismological Center (ISC) bulletin. We gathered polarities from the International Seismological Summary (ISS) for the 1955 event. In this study, we employed three programs, FOCMEC, HASH, and PINV, included in Seisan software version 2.5 (Havskov et al., 2020) to invert the polarity data and provide the optimum focal mechanism solutions of the studied earthquakes (Table 2). These solutions were computed using the velocity models MC, which cover the structures for the investigated area (Marzouk and Makris, 1990). This model is composed of three layers: an upper layer has a thickness of 7 km, a middle layer has a thickness of 11 km, and the lower layer has a thickness of 12 km, the P-wave velocities of the three layers are 4.5, 6.0 and 6.5 km/s respectively. The velocity of the upper mantle is 8.0 km/s. We created a polarity-based initial fault plane solution using the PINV software of Suetsugu, 1998. FOCMEC was used to perform a grid search based on this solution to find alternative solutions depending on the selected number of polarity data errors. Our solutions were estimated using a 3° grid search, and we selected the one that gives a good separation of the polarity data with the minimum polarity errors. The software of HASH (Hardebeck and Shearer 2002, 2008) led us to produce solutions with less than a specified number of P-waves polarity errors and less than the specific S/P amplitude ratio errors limit. In this study, we used only P-waves polarity data. The best solution was the one that automatically fits the observed polarity data taking into consideration the polarity errors. The key advantage of HASH is that it automatically seeks just one or a limited number of the most appropriate solutions, as opposed to

Table 2. Parameters of the focal mechanism's solutions located at the Egyptian continental margin using PINV, FOCMEC, HASH.

No.	YYYYMMDD	Location		Mag	Fault plane solution			P-axis		T-axis		B-axis		Software used	SH-Az	Fault type
		Lat.	Long.		M_L	Strike	Dip	Rake	Trend	Plunge	Trend	Plunge	Trend			
1	19510130	32.3725	33.4537	5.6	259.00	55.00	-151.00	117.00	43.00	208.00	06.00			FOCMEC		
					274.00	60.00	-142.00	128.00	46.00	38.00	01.00	306.00	43.00	HASH	128.00	NS
2	19550912	32.4183	29.7483	6.2	223.00	68.00	27.93	352.56	05.00	84.52	33.85			FOCMEC		
					220.00	67.00	31.00	348.00	03.00	80.00	38.00			PINV		
					241.00	70.56	34.17	007.90	08.07	104.15	37.52	267.0	51.32	HASH	007.00	SS
3	19870409	32.4493	29.0268	4.4	288.00	78.00	163.40	336.00	03.00	244.00	19.00			FOCMEC		
					92.00	57.00	159.00	320.00	10.00	58.00	37.00			PINV		
					284.00	88.00	164.00	330.00	09.00	238.00	12.00	97.00	73.00	HASH	330.00	SS
4	19880609	32.1630	27.9509	4.5	273.00	59.00	140.00	329.00	03.00	238.00	47.99			FOCMEC		
					322.00	68.00	180.00	185.00	15.00	280.00	15.00			PINV		
					293.00	60.00	151.00	165.00	03.00	257.00	40.57	71.00	49.00	HASH	165.00	TS
5	19980528	31.4010	27.6670	5.9	125.00	30.00	94.00	33.00	15.00	205.00	75.00	302.00	02.00	FOCMEC		
					120.00	42.00	85.00	33.00	03.00	286.00	86.00			PINV		
					136.0	34.00	96.00	41.00	11.00	205.00	8.00	311.00	3.00	HASH	41.00	TF
6	20121019	32.5770	30.9775	5.1	130.00	80.06	05.00	085.00	03.00	354.00	11.00			FOCMEC		
					137.00	77.00	-01.00	093.00	10.00	01.00	08.00			PINV		
					139.34	71.00	01.00	95.00	12.00	02.00	14.00	225.00	70.00	HASH	95.00	SS
7	20130117	32.0268	30.6412	4.8	145.04	73.00	17.00	277.00	00.00	08.00	24.00			FOCMEC		
					146.00	61.00	12.00	101.00	12.00	04.00	28.00			PINV		
					148.00	61.00	22.00	99.00	05.19	05.81	35.00	196.00	54.00	HASH	99.00	SS
8	20150903	30.6164	28.4589	4.2	257.00	60.00	-151.00	113.00	39.79	206.15	03.00			FOCMEC		
					269.00	70.00	-176.00	132.00	17.00	225.00	11.00			PINV		
					259.00	63.00	-161.10	118.00	31.00	212.00	06.00	312.00	57.00	HASH	302.00	SS
9	20190515	32.7803	32.5889	5.1	138.00	84.00	07.00	273.00	01.00	03.00	09.00			FOCMEC		
					138.00	81.00	-11.00	094.00	15.00	185.00	01.00			PINV		
					141.00	81.00	00.00	096.00	06.00	05.00	06.00	227.00	80.00	HASH	096.00	SS
10	20190705	32.4543	30.8282	4.8	321.00	78.00	-176.00	275.00	06.00	185.00	11.00			FOCMEC		
					311.00	76.00	-28.00	267.00	30.00	02.00	09.00			PINV		
					312.00	78.00	-2.00	267.00	10.00	176.6	07.00	52.00	78.00	HASH	267.00	SS
11	20200411	31.5567	26.8932	4.3	304.00	68.00	-145.00	165.00	39.00	70.00	06.00			FOCMEC		
					303.00	80.00	-164.00	168.00	18.00	76.00	04.00			PINV		
					302.00	63.00	-156.00	160.00	35.00	253.00	03.00	347.00	54.49	HASH	343.00	SS

FOCMEC, in which one solution must be manually selected from various alternatives. Hash software computes takeoff angles and ray azimuths for a specific event location and velocity model and conducts a grid search of possible focal mechanism solutions. The first step begins by recognizing the mechanisms that reduce the number of impulsive polarity mismatches. The subset that minimizes the number of misfit emerging polarities is selected if numerous mechanisms suit all impulsive polarities. All acceptable solutions are compiled in a list. The cluster with the most acceptable mechanisms will likely include the best solution. It is identified by averaging the acceptable alternatives after eliminating outliers. Averaging the vector coordinates of the normal to the nodal planes yields the average solution. When all of the remaining mechanisms are within 30° of the average, we iteratively eliminate the one that is the furthest away from the average and then calculate a new average. The group of acceptable solutions for each earthquake is used to describe the confidence regions nonparametrically for each earthquake. The solution is considered stable regarding possible errors if acceptable mechanisms are clustered around the preferred mechanism. The root-mean-square (RMS) angular difference between the acceptable and favoured mechanisms serves as a measure for the spread of the solutions. When a brief representation is required, the RMS rotation angle can be utilized as the 1σ mechanism uncertainty. RMS uncertainty is defined as:

$$rms_diff = \sqrt{\sum_{i=1}^n \frac{(\Delta Y_i)^2}{n}},$$

where ΔY_i is the rotation angle of the i - the acceptable solution (plane) into the average (preferred) one.

The focal solutions from PINV, FOMEC, and HASH software for the eleven earthquakes in the Egyptian continental margin were plotted as shown in Figs. 3 and 4, and Tab. 2. To measure the compatibility between the solutions resulting from FOMEC and HASH codes, we calculated the Kagan angle, which quantifies how much one double-couple earthquake source should rotate for it to coincide with another (Kagan, 1991). This angle may be between 0° , which denotes complete agreement between the two solutions, and 120° , which indicates total disagreement. Kagan's angle less than about 20° – 25° indicates a minor difference (Ponderal et al., 2006). The estimated Kagan's angle for the eleven solutions is given in Tab. 3. We calculated the other uncertainty parameters, including the weighted fraction of polarity misfits, fault plane uncertainty, and station distribution ratio by HASH software (Tab. 3), beside the azimuth and the takeoff angle gap. The maximum takeoff angle gap needs to be less than 60° . This implies that not all takeoff angles can be close to horizontal or vertical. Then, we could detect the quality factors for each event based on the calculated uncertainty parameters.

Table 3. Quality parameters are calculated by HASH software.

Event N ^o / YYYYMMDD	RMS Fault plane uncertainty	Weighted fraction of pol. misfits	Station distribution ratio (STDR)	Azimuth gap	N ^o of polarities	Quality degree according to Kilb and Hardebeck (2005)	Kagan angle
1/19510130	52.60	0.09	0.67	280	12	E	13.61
2/19550912	29.80	0.20	0.74	40	45	B	30.11
3/19870409	27.60	0.11	0.67	186	28	E	10.80
4/19880609	07.55	0.03	0.79	116	46	A*	9.39
5/19980528	22.40	0.03	0.74	85	54	A	1.0
6/20121019	20.05	0.08	0.84	37	105	A	14.0
7/20130117	20.35	0.11	0.82	42	48	A	13.0
8/20150903	21.75	0.03	0.67	63	42	A	11.5
9/20190515	16.00	0.14	0.78	47	65	A	8.5
10/20190705	13.55	0.15	0.55	76	46	A	20.38
11/20200411	21.60	0.10	0.59	63	42	A	11.47

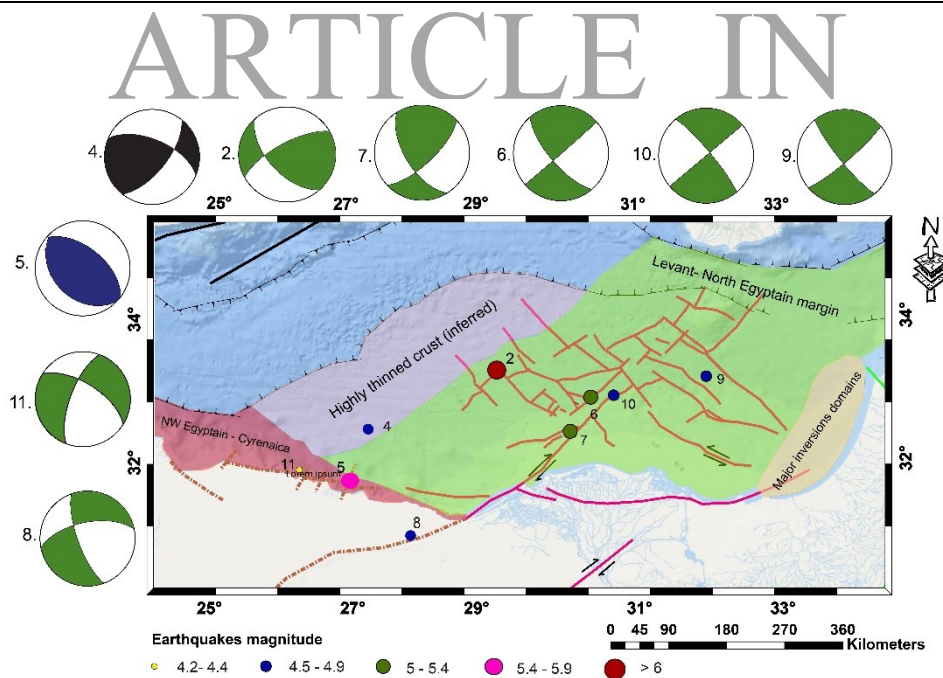


Figure 3. The map shows the earthquake focal mechanism with a quality factor range of A to D on the Egyptian continental margin and within the Mediterranean basin. Event N^o. 4 occurred on a thrust fault with slight strike-slip component, event N^o. 5 is pure thrust fault one, events N^o. 2, 6, 7, 8, 9, 10, 11 are strike-slip).

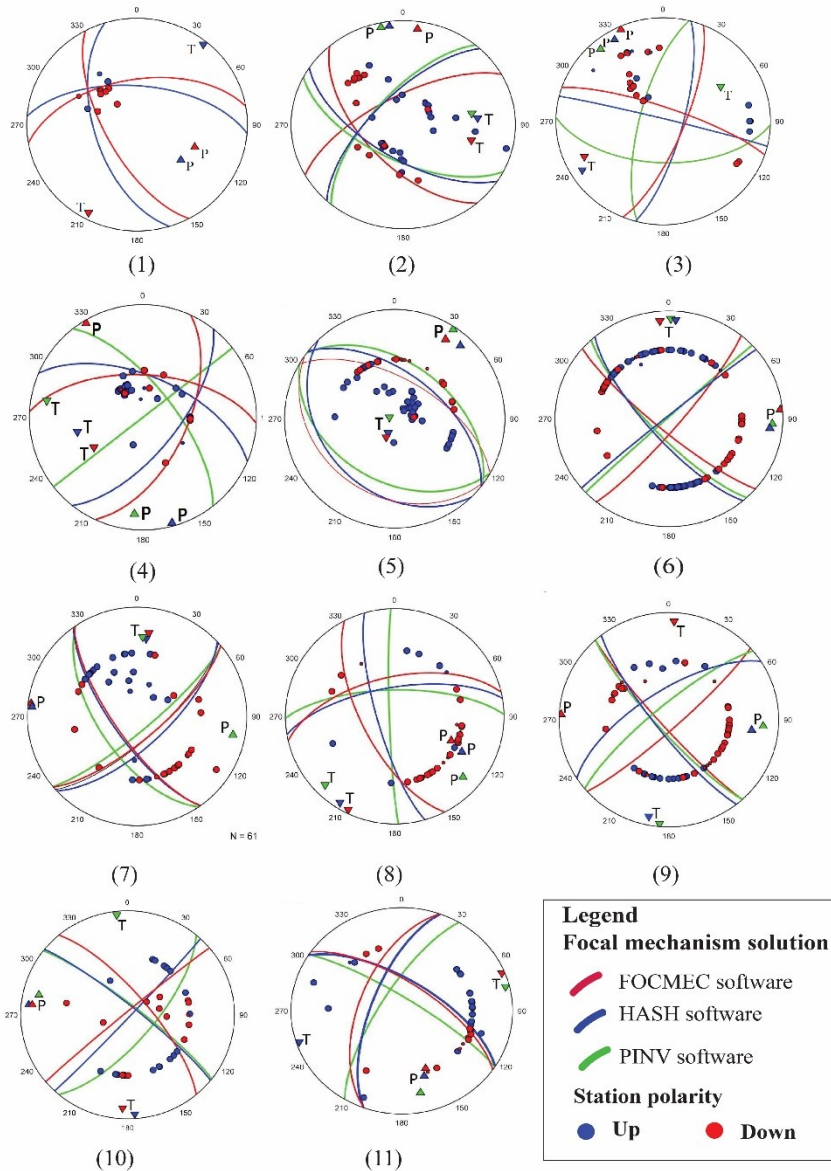


Figure 4. The best-fitted nodal planes for the polarity distribution of the constructed focal mechanism solutions (Tab. 3).

The quality control factors are assumed to depend on the initial tests done by (Kilb and Hardebeck, 2006) of the best indicators to detect the best mechanism solutions from the alphabetic letter 'A' as the best sequence to the

letter 'F' for bad solutions. One of these indicators is the station distribution ratio (STDR). STDR is a measure of the distribution of data on the focal sphere concerning the radiation pattern (Reasenber and Oppenheimer, 1985). This ratio is less than 0.5 when numerous data are located close to the nodal planes in the solution. Such a solution should be carefully reviewed before being rejected or accepted because it is less reliable than the one for which $STDR > 0.5$. According to Kilb and Hardebeck, 2006, the root mean square error (RMS) of the fault plane uncertainty has been considered the best single parameter indicator of mechanism quality and was calculated as $0.5 \times (rms_diff(1) + rms_diff(2))$. The best mechanism has been obtained when this value is less than 35° . Here $rms_diff(1)$, and $rms_diff(2)$ are the angular differences between the preferred average plane and all other acceptable planes (1 = fault plane, 2 = auxiliary plane). The misfit function is an additional uncertainty parameter, the percentage of weighted misfit polarities. Therefore, a perfect fit to data corresponds to 0% (or 0.0) and an ideal misfit to 100% (or 1.0). The search procedure, which selected a collection of acceptable nodal planes based on the earth's velocity structure and estimated takeoff angles, reduced the number of impulsive polarity mismatches (Lentas, 2018). The quality grade of the HASH software is quantified based on the following criteria (Hardebeck and Shearer, 2002):

- a) Quality A: A RMS difference of the fault planes $\leq 25^\circ$, misfit percentage ≤ 0.15 of polarities, and station distribution ratio $STDR \geq 0.5$.
- b) Quality B: A RMS difference of the fault planes $\leq 35^\circ$, misfit percentage ≤ 0.20 of polarities, and station distribution ratio $STDR \geq 0.4$.
- c) Quality C: A RMS difference of the fault planes $\leq 45^\circ$, misfit percentage ≤ 0.30 of polarities, and station distribution ratio $STDR \geq 0.3$.
- d) Quality D: All others
- e) Quality E: Solutions with a maximum azimuthal gap $> 90^\circ$.

5. Results

FOMEC and HASH software provided just similar focal mechanism solutions for most events. Comparing the solutions from both software based on the Kagan angle, we observed that this angle is less than 21 for the eleven focal mechanism solutions. This value indicated that the solutions derived by the two programs for the same event are compatible. This study addressed solutions derived from the HASH code because it assessed uncertainties quantitatively. In summary, eight focal mechanism solutions acquired an A grade, two E grades, and only one event acquired a B grade (Tab. 3). The January 30, 1951, and April 09, 1987 mechanisms (Events N^o 1 and N^o 3 Tab. 2 and Fig. 4), which had an E rating, were eliminated from the data set in (

Fig. 3). We graded the quality of the focal mechanism solutions using the quality parameters of Hardebeck and Shearer (2002). The focal mechanism solutions of events № 5, 6, 7, 8, 9, 10, and 11 received grade A (Tab. 3) which is attributed to the following conditions: 1) The percentage of misfit polarities is close to zero (≤ 0.15), polarity data are well fitted; 2) a large number of polarity data are positioned away from the fault planes ($STDR > 0.5$); 3) the average difference between the preferred plane and the other acceptable planes (misfit) is less than 25° . Event № 4 fulfilled all the conditions of grade A, except for the azimuth gap, which showed a higher value ($gap = 116^\circ$, Tab. 3) than that suggested by Hardebeck and Shearer (2002) ($gap \leq 90^\circ$). However, the two fault planes are well controlled, and the gap is close to the threshold value. Therefore, we assigned it a provisional A* grade ((A) in Tab. 3). The criteria of azimuthal gap $> 90^\circ$ resulted in an E rating for events № 1 and 3, which reflected a significant azimuthal gap (Tab. 3).

According to the different slip movements, we categorized the remaining ten events. According to the tectonic regime assignment of Zoback, 1992, all available solutions in the Egyptian continental margin showed that there are three main types of focal mechanism solutions, including the pure reverse faulting mechanism (Event № 5, Tab. 2 and Figs. 3 and 4), the strike-slip faulting mechanism (Events № 2, 6, 7, 8, 9, 10, and 11; Tab. 2 and Figs. 3 and 4) and strike-slip with some thrust component (Event № 4; Tab. 2 and Figs. 3 and 4). The event of the first type (Event № 5; Tab. 2 and Figs. 3 and 4) is located in the Levant-north Egyptian continental margin domain, on the periphery of the continental shelf, with two planes striking NNW-SSE and dipping in the direction of NE and SW, respectively. The majority of the second-type events (Events № 2, 6, 7, 9, and 10) occurred in the Levant-north Egyptian continental margin region, together with the third type (Event № 4). The first event of the second type (Event № 2) is located in the vicinity of the eastern border of the Herodotus basin. This event displayed fault planes trending NE-SW and NW-SE and dipping towards the NW and SW, respectively. Another group of the second type events (Events № 6, 7, 9, and 10) east of the Rosetta fault zone are similar, with two steeply dipping planes trending NW-SE and NE-SW. The third type of event (Event № 4) occurred within the Herodotus basin. This event showed nodal planes-oriented NE-SW and ESE-WNW and dipping towards SE and NNE, respectively.

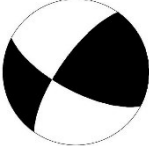
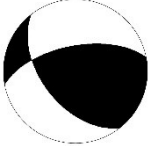
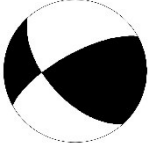
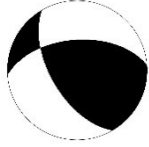
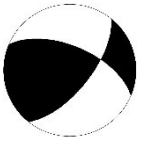
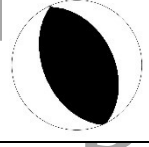
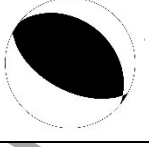
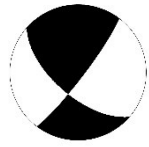
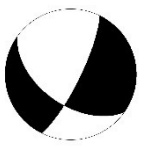
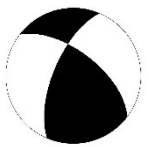
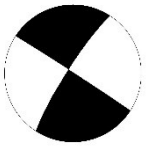
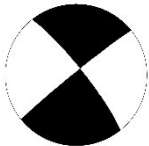
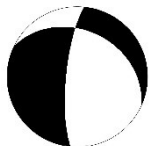
The focal mechanism solution of 2015 and 2020 events (Events № 8 and 11; Figs. 3 and 4, Tab. 2) which occurred along the Alamein fault, which represents the extension of the Rosetta-Qattara extension in the Western Desert, and the NW Egyptian-Cyrenaica margin domain, respectively, exhibited prevalently strike-slip faulting mechanisms with a normal component. The solution of the first event manifested two planes trending ENE-WSW and NNW-SSE, while the nodal planes in the second event strike NNE-SSW and WNW-ESE.

6. Discussion

We constructed the focal mechanisms for eleven earthquakes along the Egyptian continental margin between 1951 and 2020, with local magnitudes M_L ranging from 4.2 to 6.2. Nine of these solutions were assigned quality grades A and B in this study; however, the mechanisms of the 1951 and 1987 earthquakes were of E quality grade because of the large azimuthal gap brought on by inadequate station coverage at that time. Consequently, we ignored this solution.

The earthquake group located within the Levant-north Egyptian margin domain to the east of the Rosetta fault zone manifested a strike-slip faulting mechanism, with the dominant compressional direction trending nearly E-W. The SH max orientations obtained from borehole breakouts below evaporites in this region of the domain showed orientations approximately E-W to ENE-WSW (Tingay et al., 2011). The group of events in this region includes four events with two nodal planes trending NNE-SSW and NNW-SSE. Three of these mechanisms occurred within the Rosetta-Qattara fault zone and include the October 19, 2012, January 17, 2013, and July 5, 2019, events. The plane trending NNE-SSW is consistent with the trend of faults in this zone. This plane showed right-lateral strike-slip motion. The same sense of motion appeared during the Early Miocene along the same fault (Hanafy et al., 2017). Our solutions for the October 19, 2012, and January 17, 2013, earthquakes agreed with those of Badreldin et al. 2018 (Tab. 4) with the two planes of the second one having opposite dip directions. They analyzed both events using the PMAN software developed by Suetsugu, in 1998. However, the findings of Badawy et al. (2015) for both events (Tab. 4), derived from the moment tensor inversion of a few seismograms from local stations, showing a dip-slip normal motion, directly contradicted the abovementioned results. The focal solution for the October 19, 2012 event constructed by Hassoup et al. (2016) using FOCMEC software (Tab. 4) differed slightly from the results obtained in this study. Their solution showed a combination of reverse and strike-slip motions instead of strike-slip motion. Previous studies did not evaluate uncertainties associated with the focal mechanism solutions. Our solutions related to the azimuth gap are smaller than in the previous studies since we incorporated in our investigation additional stations from local and regional distances. The mechanism of the earthquake on October 19, 2012, which occurred along the NNW-SSE trending fault in the sub-linear Tamsah fault shear zone, represents the fourth mechanism in the region to the east of the Rosetta fault. We believe that the plane trending NNW-SSE represents the actual fault plane. This fault plane shows a sinistral strike-slip sense of motion. This sense of motion was similar to that of El Barkooky and Helal (2002).

Table 4. Comparison of focal mechanisms published by other authors and those from this work.

Earthquake date YYYYMMDD		19550912		
Authors	Constantinescu et al. (1996)	Korrat et al. (2005)	In this study	
Focal mechanism solutions				
Earthquake date YYYYMMDD		19880609		
Authors	Korrat et al. (2005)	In this study		
Focal mechanism solutions				
Earthquake date YYYYMMDD		19980528		
Authors	Abou Elenean and Hussein (2007)	In this study		
Focal mechanism solutions				
Earthquake date YYYYMMDD		20121019		
Authors	Badreldin et al. (2019)	Badawy et al. (2015)	Hassoup et al. (2016)	In this study
Focal mechanism solutions				
Earthquake date YYYYMMDD		20130117		
Authors	Badreldin et al. (2019)	Badawy et al. (2015)	In this study	
Focal mechanism solutions				

Within the Herodotus basin and areas close to its eastern border, which is a part of the Levant-North Egyptian Margin domain, the focal mechanism

solutions showed a strike-slip faulting mechanism or strike-slip mechanism with some thrust component, exhibiting a dominant compressional orientation trending NNW-SSE to NNE-SSW. This group includes September 12, 1955, and June 9, 1988. The focal mechanisms of the first event displayed ENE/SES trends for the direction of the nodal plane strike. For the event on September 12, 1955, the solution of Constantinescu et al., 1966 provided the same type of mechanism that was compatible with our solutions with only minor changes in the strike of both planes (Table 4), while the solution of Korrat et al. (2005) for the same event displayed a thrust faulting mechanism with a strike-slip component and only one plane rotated to the east in comparison to our solution (Tab. 4). The NNE-SSW direction of the compressional axis calculated from the September 12, 1955 event's focal mechanism was compatible with the SH max reported in the WSM database (Heidbach et al., 2018) for the same event.

The solution provided by Korrat et al. (2005) for the June 9, 1988 event displayed the same type of faulting mechanism identified in the present study, with the nodal planes being oriented differently (Tab. 4). May 5, 1998, M_L 5.9 event, located on the periphery of the continental shelf of the same Margin domain and to the south of the two events mentioned above, displayed a thrust faulting mechanism. However, the derived compressional axis orientation has been changed to ENE-WSW. This compressional axis is consistent with the one achieved by Tingay et al. (2012) from drilling-induced Fractures and borehole breakouts in the same zone of the 1998 earthquake. The solution provided by Abou Elenean et al. (2007) for the 1998 event manifested a similar solution to our findings (Tab. 4).

The only event within the NW Egypt-Cyrenaica margin domain was the April 11, 2020, earthquake. This event manifests strike-slip faulting mechanisms. The NW-SE trending plane closely follows the narrow, highly faulted zone that separates the continental shelf from the oceanic crust that underlies the Herodotus and Ionian abyssal plains. This transcurrent fault zone displays right-lateral strike-slip motion. On September 3, 2015, one more strike-slip event occurred along the Alamein fault, an extension of the NE trending Rosetta-Qattara fault zone in the Western desert. The motion along this fault trend identified from the focal mechanism solution is the right lateral strike-slip motion.

7. Conclusions

The focal mechanism solutions derived from the polarity data of ten earthquakes in the passive Egyptian continental margin were to find the distribution of the different types of faulting in the two main domains of the margin, the Levant-north Egyptian margin and the NW Egypt-Cyrenaica margin. We get the following results:

1. The examination of the focal mechanism solutions in the Levant-north Egyptian domain reveals strike-slip faulting with only a single event involving a thrust component, implying that this domain can be divided into two sub-provinces with different stress orientations. These sub-provinces are the region east of the Rosetta fault zone and Herodotus Basin - its adjacent eastern region.
2. The focal mechanism solutions in the first sub-province reflect strike-slip faulting on planes trending NW and NE, which corresponds to the directions of the two main strike-slip faults in the region; the NE trending Rosetta-Qattara and the NW trending Tamsah fault zones. This type of motion is generated from the collision of the Cyprian Arc with the Eratosthenes Seamount, which transmits plate boundary stress southward and reactivates the pre-existing NW and NE strike-slip fault zones. This implies that the orientation of the pre-existing faults has an impact on the stress field as well. Similar to those observed in the borehole breakout data below evaporites, all of the events in this sub-province have pressure axes that fall between E-W and ENE-WSW directions. These events manifest deep-seated tectonics in contrast to salt tectonics.
3. The focal mechanism solution of a single earthquake along the Alamein fault, which marks the continuation of the NE trending Rosetta-Qattara fault through the Western Desert, also shows the same type of motion that causes deformation along the Rosetta-Qattara fault.
4. The focal mechanism solutions of the earthquakes that struck the Herodotus basin and its neighbouring eastern regions, which constitute the second sub-province, generally correspond to strike-slip faulting or strike-slip with thrust component. The geologic analysis, in full conformity with the focal mechanism solution, suggests that the NW to NNW tectonic compression is the main stress orientation in the Herodotus basin.
5. The first and the second sub-provinces of the Levant-north Egyptian margin have different orientations of compressional stress due to variations in the nature of convergence along the Hellenic and Cyprian arcs as a result of their complex geometries as well as the effects of the local structure characteristics which reconfigure the regional stress field.
6. The source mechanism of the 1998 event, located in the periphery of the continental shelf, manifests a pure thrust mechanism that reflects compressional stress. The NNE-SSW direction of the SHmax calculated from breakout data in the same zone coincides well with the P-axis trend deduced from the focal mechanism solution. This compressional stress trend rotates clockwise in comparison to what was observed in the Herodotus basin. A probable interpretation of the 1998 event focal mechanism is that the Hellenic Arc southwestward retreat generated

movement that transmitted stress to the south, which consequently caused intraplate compressional stress, which caused such type of tectonic deformation.

7. The focal mechanism solution of a single event in the NW Egypt-Cyrenaica margin of the second domain suggests NW trending strike-slip deformation, consistent with that along the NW trending transcurrent fault zone that separates the continental shelf from the oceanic crust underlying the Herodotus and Ionian abyssal plains.

Data availability – All used data and related results of this article are presented in the paper.

Author contributions – MA collected and analyzed the seismicity and focal mechanism data, AS and MA prepared and analyzed tectonics maps, ME wrote the manuscript, HH, AS, and IA provided interpretation and discussion, and HH and IA reviewed the manuscript.

Acknowledgements – The National Research Institute of Astronomy and Geophysics-NRIAG, Helwan, Cairo, Egypt, supported this work. The authors, therefore, acknowledge with thanks NRIAG's technical support. We are grateful to the Egyptian National Seismological Network, the International Data Center of the Comprehensive Test Ban Treaty Organization, and the International Seismological Centre (ISC) for providing the seismological data.

References

- Abdel-Aal, A., El Barkooky, A., Gerrits, M., Meyer, H., Schwander, M. and Zaki, H. (2000): Tectonic evolution of the Eastern Mediterranean Basin and its significance for hydrocarbon prospectively in the ultra-deepwater of the Nile Delta, *The Leading Edge*, **19**, 1086–1102, <https://doi.org/10.1190/1.1438485>.
- Abdel-Aal, A., El Barkooky, A., Gerrits, M., Meyer, H.-J., Schwander, M. and Zaki, H. (2001): Tectonic evolution of the Eastern Mediterranean basin and its significance for hydrocarbon prospectivity of the Nile Delta Deep Water Area, *GeoArabia*, **6**(3), 363–383, <https://doi.org/10.2113/geoarabia0603363>.
- Abd El-Fattah, B. K., Yousef, M., and Moustafa A. R. (2018): 2D structural restoration of the Rosetta fault system, offshore western Nile Delta, Mediterranean basin, Egypt, *J. Appl. Geophys.*, **17**, 83–98.
- Abd El-Fattah, B. K., Moustafa, A. R. and Yousef, M. (2021): A new insight into the structural evolution of Rosetta Fault, eastern margin of Herodotus Basin, East Mediterranean, *Mar. Petrol. Geol.*, **131**, 105161, <https://doi.org/10.1016/j.marpetgeo.2021.105161>.

- Abou Elenean, K. M. and Hussein, H. M. (2007): Source mechanism and source parameters of May 28, 1998 earthquake, Egypt, *J. Seismol.*, **11**, 259–274, <https://doi.org/10.1007/s10950-007-9051-5>.
- Ambraseys, N. N., Melville, C. P. and Adams, R. D. (2005): *The seismicity of Egypt, Arabia and the Red Sea: A historical review*. Cambridge University Press, 181 pp.
- Badawy, A., Mohamed G., Omar, K., and Faried, W. (2015): The northern Egyptian continental margin, *J. Afr. Earth Sci.*, **101**, 177–185, <https://doi.org/10.1016/j.jafrearsci.2014.09.009>.
- Badreldin, H., Abd el-aal, A. K., Toni, M. and El-Faragawy, K. (2018): Moment tensor inversion of small-to-moderate size local earthquakes in Egypt, *J. Afr. Earth Sci.*, **151**, 153–172, <https://doi.org/10.1016/j.jafrearsci.2018.12.004>.
- Barrier, E., Chamot-Rooke, N., and Giordano, G. (2004): Geodynamic maps of the Mediterranean – sheet 1: Tectonics and kinematics, Commission for the Geological Map of the World (CGMW) & UNESCO, 1 sheet: 99 cm × 53 cm, 1:13.000.000 scale.
- Ben-Avraham, Z., and Nur, A. (1987): Effects of collisions at trenches of oceanic ridges and passive margin, in: *Circum-Pacific orogenic belts and evolution of the Pacific Ocean 406 basins*, edited by: Monger, J. W. H. and Francheteau, J. American Geophysical Union, Geodynamics Series, **18**, 9–18.
- Ben-Avraham, Z., Ginzburg, A., Makris, J. and Eppelbaum, L. (2002): Crustal structure of the Levant Basin, eastern Mediterranean, *Tectonophysics*, **346**(1–2), 23–43, [https://doi.org/10.1016/S0040-1951\(01\)00226-8](https://doi.org/10.1016/S0040-1951(01)00226-8).
- Bird, D. (2001): Shear margins: Continent-ocean transform and fracture zone boundaries, *The Leading Edge*, **20**, 150–159, <https://doi.org/10.1190/1.1438894>.
- Brönnner, M. and Makris J. (2000): Crustal structure of the Libyan margin, in: *Proceedings of the African continental margins of the Mediterranean Sea*, Djerba, Tunisia, 22–25 November 2000, CISEM Workshop Series No. **13**, 63–66.
- Brune, S., Heine, C., Pérez-Gussinyé M. and Sobolev, S. V. (2014): Rift migration explains continental margin asymmetry and crustal hyper-extension, *Nat. Commun.*, **5**, 4014, <https://doi.org/10.1038/ncomms5014>.
- Caméra, L., Ribodetti, A. and Mascle, J. (2010): Deep structures and seismic stratigraphy of the Egyptian continental margin from multichannel seismic data, *Geol. Soc. Spec. Publ.*, **341**, 85–97, <https://doi.org/10.1144/SP341.5>.
- Constantinescu, L., Ruprechtova, L. and Enescu, D. (1966): Mediterranean-Alpine earthquake mechanisms and their seismotectonic implications, *Geophys. J. Int.*, **10**(4), 347–368.
- Courtillot, V., Armijo, R. and Tapponnier, P. (1987): The Sinai triple junction revisited, *Tectonophysics*, **141**(1–3), 181–190, [https://doi.org/10.1016/0040-1951\(87\)90184-3](https://doi.org/10.1016/0040-1951(87)90184-3).
- Cowie, L. and Kusznir, N. (2012a): Mapping crustal thickness and oceanic lithosphere distribution in the Eastern Mediterranean using gravity inversion, *Petrol. Geosci.*, **18**, 373–380, <https://doi.org/10.1144/petgeo2011-071>.

- Cowie, L. and Kusznir, N. (2012b): Gravity inversion mapping of crustal thickness and lithosphere thinning for the eastern Mediterranean, *The Leading Edge*, **31**, 810–814, <https://doi.org/10.1190/tle31070810.1>.
- Dolson, J. C., Atta, M., Blanchard, D., Sehim, A., Villinski, J., Loutit, T. and Romine, K. (2014): Egypt's future petroleum resources: A revised look into the 21st century, in: *Petroleum systems of the Tethyan region*, edited by Marlow, L., Kendall, C. and Yose, L. AAPG Memoir, **106**, 143–178, <https://doi.org/10.1306/13431856M106713>.
- El Barkouky, A. and Helal, M. (2002): Some Neogene stratigraphic aspects of the Nile Delta, Mediterranean Offshore Conference (MOC, 2002), Alexandria, Egypt, 7–9 April 2002, 35 pp.
- Eyal, Y. and Reches, Z. (1983): Tectonics analysis of the Dead Sea rift region since late–Cretaceous based on mesostructures, *Tectonics*, **2**(2), 167–185, <https://doi.org/10.1029/TC002i002p00167>.
- El-Gabry, M. N., Panza, G. F., Badawy A. A. and Korrat, I. M. (2012): Imaging a relic of complex tectonics: The lithosphere-aesthenosphere structure in the Eastern, *Terra Nova*, **25**, 102–109, <https://doi.org/10.1111/ter.12011>.
- El-Sharkawy, A., Meier, T., Hübscher, C., Lebedev, S., Dannowski, A., Kopp, H., Behrmann, J. H., McGrandle, A. and Hamada, M. (2021): Lithospheric structure of the eastern Mediterranean Sea: Inferences from surface wave tomography and stochastic inversions constrained by wide-angle refraction measurements, *Tectonophysics*, **821**, 229159, <https://doi.org/10.1016/j.tecto.2021.229159>.
- Ghalayini, R., Daniel, J. M., Homberg, C., Nader, F. H. and Comstock, J. E. (2014): Impact of Cenozoic strike-slip tectonics on the evolution of the northern Levant Basin (offshore Lebanon), *Tectonics*, **33**, 2121–2142, <https://doi.org/10.1002/2014TC003574>.
- Hanafy, S., Nimmagadda, S. L., Mahmoud, S. E. and Mabrouk, W. M. (2017): New insights on structure and stratigraphic interpretation for assessing the hydrocarbon potentiality of the offshore Nile Delta basin, Egypt, *J. Petrol. Explor. Prod. Technol.*, **7**, 317–339, <https://doi.org/10.1007/s13202-016-0264-4>.
- Hardebeck, J. L., and Shearer, P. M. (2002): A new method for determining first-motion focal mechanisms, *Bull. Seismol. Soc. Am.*, **92**(6), 2264–2276, <https://doi.org/10.1785/0120010200>.
- Hardebeck, J. L., and Shearer, P. M. (2008): HASH: A FORTRAN program for computing earthquake first-motion focal mechanisms–v1.2 – January 31, 2008, 17 pp.
- Hassoup, A. and Tealeb, A. (2000): Attenuation of intensity in the northern part of Egypt associated with the May 28, 1998 Mediterranean earthquake, *Acta Geophys. Pol.*, **48**, 79–92.
- Hassoup, A., Toni, M., Farag, S. M., Helal, A. M. and Mohamed, E. K. (2016): Source mechanism and parameters of the 19 October 2012 earthquake, northern Egyptian continental margin, *Arab. J. Geosci.*, **9**, 313, <https://doi.org/10.1007/s12517-016-2338-5>.

- Havskov J., Voss, P. H. and Ottemoller, L. (2020): Seismological Observatory Software: 30 Yr of SEISAN, *Seismol. Res. Lett.*, **91**(3), 1846–1852, <https://doi.org/10.1785/0220190313>.
- Heidbach, O., Rajabi, M., Reiter, K., Ziegler, M. O. and the WSM Team (2016): World Stress Map database release 2016. GFZ Data Services. <https://doi.org/10.5880/WSM.2016.001>.
- Heidbach, O., Rajabi, M., Cui, X., Fuchs, K., Müller, B., Reinecker, J., Reiter, K., Tingay, M., Wenzel, F., Xie, F., Ziegler, M. O., Zoback, M. L. and Zoback, M. D. (2018): The World Stress Map database release 2016: Crustal stress pattern across scales, *Tectonophysics*, **744**, 484–498, <https://doi.org/10.1016/j.tecto.2018.07.007>.
- Holdsworth, R. E., Hand, M., Miller, J. A. and Buick, I. S. (2001): Continental reactivation and reworking: An introduction, *Geol. Soc. Spec. Publ.*, **184**, 1–12, <https://doi.org/10.1144/GSL.SP.2001.184.01.01>.
- Huguen, C., Chamot-Rooke, N., Loubrieu, B. and Mascle, J. (2006): Morphology of a pre-collisional, salt-bearing, accretionary complex: The Mediterranean Ridge (Eastern Mediterranean), *Mar. Geophys. Res.*, **27**, 61–75, <https://doi.org/10.1007/s11001-005-5026-5>.
- Hussein, M. A. E. (2013): 3D Seismic reflection and well log data analysis for reservoir characterization at Oligocene sands, Nile Delta, Egypt. MSc Thesis, Ain Shams University, 208 pp.
- Jagger, L. J., Bevan, T. G. and McClay, K. R. (2018): Tectonostratigraphic evolution of the SE Mediterranean passive margin, offshore Egypt and Libya, *Geol. Soc. Spec. Publ.*, **476**, 365–401, <https://doi.org/10.1144/SP476.10>.
- Johnston, A. C. (1989): The seismicity of ‘Stable Continental Interiors’, in: *Earthquakes at North-Atlantic Passive Margins: Neotectonics and Postglacial Rebound. NATO ASI Series (Series C: Mathematical and Physical Sciences)*. Springer, Dordrecht, **266**, 299–327, https://doi.org/10.1007/978-94-009-2311-9_18.
- Kagan, Y. Y. (1991): 3-D rotation of double-couple earthquake sources, *Geophys. J. Int.*, **106**(3), 709–716, <https://doi.org/10.1111/j.1365-246X.1991.tb06343.x>.
- Kempler, D. (1998): Eratosthenes Seamount: the possible spearhead of ancient continental collision in the Eastern Mediterranean, in: *Proceedings of the Ocean Drilling Program. Scientific Results*, edited by Robertson, A. H. F., Emeis, K. C., Richter, C. and Camerlenghi, A. **160**, 709–721.
- Korrat, I. M., El Agami, N. L., Hussein, H. M. and El-Gabry, M. N. (2005): Seismotectonics of the passive continental margin of Egypt, *J. Afr. Earth Sci.*, **41**, 145–150, <https://doi.org/10.1016/j.jafrearsci.2005.02.003>.
- Kilb, D., and Hardebeck, J. L. (2006): Fault parameter constraints using relocated earthquakes: Validation of first motion focal mechanism data, *Bull. Seismol. Soc. Am.*, **96**(3), 1140–1158, <https://doi.org/10.1785/0120040239>.
- Le Pichon, X. and Gaulier, J. M. (1988): The rotation of Arabia and the Levant fault system, *Tectonophysics*, **153**, 271–294, [https://doi.org/10.1016/0040-1951\(88\)90020-0](https://doi.org/10.1016/0040-1951(88)90020-0).

- Le Pichon, X., Chamot-Rooke, N., Lallemand, S., Noomen, R. and George, V. (1995): Geodetic determination of the kinematics of central Greece with respect to Europe: Implications for eastern Mediterranean tectonics, *J. Geophys. Res.*, **100**(B7), 12675–12690, <https://doi.org/10.1029/95JB00317>.
- Lentas, K. (2018): Towards routine determination of focal mechanisms obtained from first motion P-wave arrivals, *Geophys. J. Int.*, **212**(3), 1665–1686, <https://doi.org/10.1093/gji/ggx503>.
- Loncke, L., Gaullier, V., Mascle, J., Vendeville, B. and Camera, L. (2006): The Nile deep-sea fan: An example of interacting sedimentation, salt tectonics, and inherited subsalt paleotopographic features, *Mar. Petrol. Geol.*, **23**, 297–315, <https://doi.org/10.1016/j.marpetgeo.2006.01.001>.
- Maamoun, M., Megahed, A. and Allam, A. (1984): Seismicity of Egypt, *Bull. HIAG*, **4**, 109–160.
- Mann, P. (2015): Passive plate margin, in: *Encyclopedia of Marine Geosciences*, edited by Harff, J., Meschede, M., Petersen, S. and Thiede, J. Springer, Dordrecht, 1–8, https://doi.org/10.1007/978-94-007-6644-0_100-2.
- Marone, F., Van Der Meijde, M., Van Der Lee, S. and Giardini, D. (2003): Joint inversion of local, regional and teleseismic data for crustal thickness in the Eurasia–Africa plate boundary region, *Geophys. J. Int.*, **154**, 499–514, <https://doi.org/10.1046/j.1365-246X.2003.01973.x>.
- Marzouk, I. and Makris, J. (1990): Deep seismic profiles in Egypt, *Bull. Int. Inst. Seismol. Eart. Eng.*, **24**, 1–40.
- Mascle, J., Benkhelil, J., Bellaiche, G., Zitter, T., Woodside, J., Loncke, L., and Prised II scientific party (2000): Marine geological evidence for a Levantine-Sinai plate a missing piece of the Mediterranean puzzle, *Geology*, **28**, 779–782, [https://doi.org/10.1130/0091-7613\(2000\)28<779:MGEFAL>2.0.CO;2](https://doi.org/10.1130/0091-7613(2000)28<779:MGEFAL>2.0.CO;2).
- Mascle, J. and Chaumillon, E. (1998): An overview of Mediterranean Ridge collisional accretionary complex as deduced from multichannel seismic data, *Geo-Mar. Lett.*, **18**(2), 81–89, <https://doi.org/10.1007/s003670050056>.
- Mascle, J., Tiphaine, Z., Bellaiche, G., Droz, L., Gaullier, V. and Loncke, L. (2001): The Nile deep sea fan: Preliminary results from a swath bathymetry survey, *Mar. Petrol. Geol.*, **18**, 471–477, [https://doi.org/10.1016/s0264-8172\(00\)00072-6](https://doi.org/10.1016/s0264-8172(00)00072-6).
- McClusky, S., Balassanian, S., Barka, A., Demir, C., Ergintav, S., Georgiev, I., Gurkan, O., Hamburger, M., Hurst, K., Kahle, H., Kastens, K., Kekelidze, G., King, R., Kotzev, V., Lenk, O., Mahmoud, S., Mishin, A., Nadariya, M., Ouzounis, A., Paradissis, D., Peter, Y., Prilepin, M., Reilinger, R., Sanli, I., Seeger, H., Tealeb, A., Toksöz, M. N. and Veis G. (2000): Global Positioning System constraints on plate kinematics and dynamics in the eastern Mediterranean and Caucasus, *J. Geophys. Res.*, **105**, 5695–5719, <https://doi.org/10.1029/1999JB900351>.
- McClusky, S., Reilinger, R., Mahmoud, S., Ben Sari, D. and Tealeb, A. (2003): GPS constraints on Africa (Nubia) and Arabia plate motion, *Geophys. J. Int.*, **155**, 126–138, <https://doi.org/10.1046/j.1365-246X.2003.02023.x>.

- McKenzie, D. (1972): Active tectonics of the Mediterranean Region, *Geophys. J. Int.*, **30**(2), 109–185, <http://doi.org/10.1111/j.1365-246X.1972.tb02351.x>.
- Moustafa, A. R. (2020): Mesozoic-Cenozoic deformation history of Egypt, in: *The geology of Egypt, regional geology reviews*, edited by Hammi, Z., EL-Barkooky, A., Martinez Frias, J., Fritz, H. and Abd EL-Rahman, Y. Springer, Cham., 253–294, https://doi.org/10.1007/978-3-030-15265-9_7.
- Moustafa, A. and Khalil, M. (1994): Rejuvenation of the eastern Mediterranean passive continental margin in northern and central Sinai: New data from the Themed Fault, *Geol. Mag.*, **131**, 435–448, <https://doi.org/10.1017/S0016756800012085>.
- Neev, D. (1975): Tectonic evolution of the Middle East and the Levantine Basin (easternmost Mediterranean), *Geology*, **3**(12), 683–686, [https://doi.org/10.1130/0091-7613\(1975\)3<683:TEOTME>2.0.CO;2](https://doi.org/10.1130/0091-7613(1975)3<683:TEOTME>2.0.CO;2).
- Nemčok, M., Rybár, S., Sinha, S. T., Hermeston, S. A. and Ledvényiová L (eds) (2016): *Transform margins: Development, controls and petroleum systems – An introduction*. Geological Society of London, Collection, 431 pp, <https://doi.org/10.6084/m9.figshare.c.3276407.v1>.
- Orwig, R. O. (1982): Tectonic framework of Northern Egypt and the Eastern Mediterranean region, *6th Exploration and Production Conference*, **1**, 193–202.
- Peace, D. G., Stieglitz, T. and Spoor, R. (2012): Imaging new opportunities and play concepts in the Adriatic Sea and Levantine Basin, *Petrol. Geosci.*, **18**, 405–416, <https://doi.org/10.1144/petgeo2011-066>.
- Reasenber, P., and Oppenheimer, D. (1985): *Fortran computer programs for calculating and displaying earthquake fault-plane solutions*. U.S. Geological Survey Open-File Report No. 85-739, 109 pp, <https://doi.org/10.3133/ofr85739>.
- Pondrelli, S., Salimbeni, S. and Perfetti, P. (2016): Moment tensor solutions for the Amatrice 2016 seismic sequence, *Ann. Geophys.*, **59**, Fast Track 5, <https://doi.org/10.4401/ag-7240>.
- Reilinger, R., McClusky, S., Vernant, P., Lawrence, S., Ergintav, S., Cakmak, R., Ozener, H., Kadirov, F., Guliev, I., Stepanyan, R., Nadariya, M., Hahubia, G., Mahmoud, S., Sakr, K., ArRajehi, A., Paradissis, D., Al-Aydrus, A., Prilepin, M., Guseva, T., Evren, E., Dmitrotsa, A., Filikov, S. V., Gomez, F., Al-Ghazzi, R. and Karam, G. (2006): GPS constraints on continental deformation in the Africa-Arabia-Eurasia continental collision zone and implications for the dynamics of plate interactions, *J. Geophys. Res. - Solid Earth*, **111**, 1–26, <https://doi.org/10.1029/2005JB004051>.
- Robertson, A. H. F. and Dixon, J. E. (1984): Introduction: Aspects of the geological evolution of the Eastern Mediterranean, *Geol. Soc. Spec. Publ.*, **17**(1), 1–74, <https://doi.org/10.1144/GSL.SP.1984.017.01.02>.
- Rosenbaum, G., Lister, G. S. and Duboz, C. (2002): Relative motions of Africa, Iberia and Europe during Alpine orogeny, *Tectonophysics*, **359**(1–2), 117–129, [https://doi.org/10.1016/S0040-1951\(02\)00442-0](https://doi.org/10.1016/S0040-1951(02)00442-0).

- Sage, L. and Letouzey, J. (1990): Convergence of the African and Eurasian plate in the eastern Mediterranean, in: *Petroleum and tectonics in mobile belts*, edited by Letouzey, J. Editions Technip, Paris, 49–68.
- Saleh, M. and Becker, M. (2015): New constraints on the Nubia-Sinai-Dead Sea fault crustal motion, *Tectonophysics*, **651**, 79–98, <https://doi.org/10.1016/j.tecto.2015.03.015>.
- Snoke, J. A., Munsey, J. W., Teague, A. G., and Bollinger, G. A. (1984): A program for focal mechanism determination by combined use of polarity and SV-P amplitude ratio data, *Earthquake Notes*, **55**, 15.
- Suetsugu, D. (1998): *Practice on source mechanism*. International Institute of Seismology and Earthquake Engineering (IISEE) Lecture Note, Tsukuba, Japan, 104 pp.
- Tassy, A., Crouzy, E., Gorini, C., Rubino, J. L., Bouroulllec, J. L. and Sapin, F. (2015): Egyptian Tethyan margin in the Mesozoic: Evolution of a mixed carbonate-siliciclastic shelf edge (from Western Desert to Sinai), *Mar. Petrol. Geol.*, **68**, Part A, 565–581, <https://doi.org/10.1016/j.marpetgeo.2015.10.011>.
- Tingay, M., Bentham, P., De Feyter, A. and Kellner, A. (2011): Present-day stress field rotations associated with evaporites in the offshore Nile Delta, *Geol. Soc. Am. Bull.*, **123**(5–6), 1171–1180, <https://doi.org/10.1130/B30185.1>.
- Tingay, M., Bentham, P., De Feyter, A., Kellner, A. (2012): Evidence for non-Andersonian faulting above evaporites in the Nile Delta, *Geol. Soc. Spec. Publ.*, **367**(1), 155–170, <https://doi.org/10.1144/SP367.11>.
- Wdowinski, S., Ben-Avraham, Z., Arvidsson, R. and Ekström, G. (2006): Seismotectonics of the Cyprian Arc, *Geophys. J. Int.*, **164**(1), 176–181, <https://doi.org/10.1111/j.1365-246X.2005.02737.x>.
- Zoback, M. L. (1992): First- and second-order patterns of stress in the lithosphere: The World Stress Map project, *J. Geophys. Res.*, **97**(B8), 11,703–11,728. <https://doi.org/10.1029/92JB00132>.

SAŽETAK

Prostorna varijacija mehanizama izvora na egipatskoj kontinentalnoj granici

Iman F. Abu El Nader, Asem Salama, Mohamed N. El-Gabry, Hesham M. Hussein i Mona Abdelazim

Prostorna varijabilnost rješenja žarišnih mehanizama u područjima sjeverozapadnog Egipta–Kirenaike i Levanta–sjevernog Egipta na egipatskoj kontinentalnoj granici istražena je na temelju polariteta prvih pomaka P-valova jedanaest potresa s lokalnim magnitudama M_L između 4,2 i 6,2. Rješenja žarišnih mehanizama u području Levanta–sjevernog Egipta odnose se na dva potpodručja s različitim geološkim svojstvima. U prvom potpodručju mehanizmima dominiraju desni lateralni rasjedi usmjereni duž rasjedne zone Rosetta-Qattara u smjeru NE, dok su u rasjednoj zoni Temsah dominantni lijevi lateralni rasjedi pružanja prema NW. Takvi rasjedi prevladavaju i u dijelu rasjedne zone Rosetta-Qattara koja se nastavlja u untrašnjost, prema Zapadnoj pustinji. Rasjedi s pomakom po pružanju s reversnom komponentom pomaka prevladavaju u drugoj potprovinciji, ali s drugačijom orijentacijom tektonskih napetosti. Na rubu kontinentalnog šelfa dogodio se potres s reversnim mehanizmom, ali s nesigurno određenim pružanjem. Takav mehanizma na toj lokaciji može se objasniti prijenosom kompresijskog naprezanja prema obali uzrokovanim ubrzanim jugozapadnim povlačenjem Helenskog rova. Složena regionalna napetost duž ciparskog i helenskog luka, lokalne strukturne značajke i dominantna orijentacija postojećeg rasjeda doprinose varijabilnom naprezanju u domeni Levanta–sjevernog Egipta. Jedan potres u drugom području, sjeverozapadnom Egiptu–Kirenaici, dogodio se na desnom lateralnom rasjedu usmjerenom prema WNW, što je u skladu s pomacima duž tektonskog rasjeda pružanja WNW koji odvaja kontinentalni šelf od oceanske kore.

Ključne riječi: egipatska kontinentalna granica, žarišni mehanizmi, rasjed Rosetta-Qattara, pasivna granica

Corresponding author's address: Iman F. Abu El Nader, General Seismology Lab, Seismology Department, National Research Institute of Astronomy and Geophysics (NRIAG), 11421 Helwan, Cairo, Egypt; tel: (+202) 255 41 100, (+202) 237 66 826; fax: (+202) 255 48020; e-mail: iman.abuelnadr@nriag.sci.eg



This work is licensed under a [Creative Commons Attribution-NonCommercial 4.0 International License](https://creativecommons.org/licenses/by-nc/4.0/).